The following publication Chenyu Yao, Qiang Wang, Yuechuan Lin, Wei Jin, Limin Xiao, Shoufei Gao, Yingying Wang, Pu Wang, and Wei Ren, "Photothermal CO detection in a hollow-core negative curvature fiber," Opt. Lett. 44, 4048-4051 (2019) is available at https://doi.org/10.1364/OL.44.004048.

Photothermal CO detection in a hollow-core negative curvature fiber

CHENYU YAO,[1] QIANG WANG, [1] YUECHUAN LIN,[2] WEI JIN, [2] LIMIN XIAO, [3] SHOUFEI GAO, [4] YINGYING WANG, [4] PU WANG, [4] AND WEI REN, [1,*]

[1]*Department of Mechanical and Automation Engineering, The Chinese University of Hong Kong, New Territories, Hong Kong*
[2]*Department of Electrical Engineering, The Hong Kong Polytechnic University, Kowloon, Hong Kong*
[3]*Advanced Fiber Devices and Systems Group, Key Laboratory of Micro and Nano Photonic Structures (MoE), Key Laboratory for Information Science of Electromagnetic Waves (MoE), Shanghai Engineering Research Center of Ultra-Precision Optical Manufacturing, Fudan University, Shanghai 200433, China*
[4]*Beijing Engineering Research Center of Laser Technology, Institute of Laser Engineering, Beijing University of Technology, Beijing 100124, China*
**Corresponding author: renwei@mae.cuhk.edu.hk*

Received XX Month XXXX; revised XX Month, XXXX; accepted XX Month XXXX; posted XX Month XXXX (Doc. ID XXXXX); published XX Month XXXX

We demonstrated the first photothermal CO sensor using a hollow-core negative curvature fiber (HC-NCF). The hollow-core fiber features a typical structure of one ring cladding containing eight nontouching capillaries to form a negative curvature core-surround. The photothermal effect in a 40-μm hollow core is induced by CO absorption at 2327 nm and detected by a Mach-Zehnder interferometer operating at 1533 nm. By using wavelength modulation spectroscopy, we achieved a normalized noise equivalent absorption (NNEA) coefficient of 4.4×10^{-8} $cm^{-1}WHz^{-1/2}$. As CO has a very slow vibrational-translational (V-T) relaxation process, we enhanced the photothermal signal by enhancing the relaxation with the water vapor additive. © 2019 Optical Society of America

http://dx.doi.org/10.1364/OL.99.099999

Gas sensors based on photothermal interferometry (PTI) usually adopt a pump-probe two-laser configuration together with an optical interferometer. In particular, gas absorption of the pump laser induces the localized heating followed by a change of the refractive index, which can be sensitively detected by interferometry of the probe light. Compared with the free-space detection [1,2], gas sensing in a hollow core fiber (HCF) enables the perfect interaction between the single-mode radiation and gas sample over a long distance [3], leading to a higher detection sensitivity and a more compact configuration.

In recent years HCF-based PTI has been extensively studied. Jin et al. [4] performed pioneering work in developing an all-fiber near-infrared acetylene sensor with a record sensitivity (2 ppb) and a dynamic range (>10^5) by performing PTI in a 11-μm hollow-core photonic bandgap fiber (HC-PBF). Using the same type of hollow-core fiber, the PTI sensors were further advanced with the Sagnac-ring interferometry [5] or the intracavity power enhancement [6]. All these gas sensors [4-6] exploited the absorption band only at 1.5 μm due to the limited infrared transmission of the silica HC-PBF. It is known that the infrared domain at 2–13 μm is more effective for gas sensing and molecular spectroscopy as many molecules have strong rovibrational bands in this spectral region. Li et al. [7] recently reported a mid-infrared PTI sensor for N_2O detection at 4.46 μm using an inner-surface-coated HCF with a core diameter of 200 μm. However, the sensor performance was limited by the relatively large core size and fiber bending noise.

Among recent innovations in optical fiber technology, hollow-core negative-curvature fiber (HC-NCF) [8,9] is a novel type of HCF that has attracted lots of attention. HC-NCF has an inverted curvature in the core wall and usually exhibits multiple transmission bands with a low transmission loss. The unique shape of the core wall impedes the phases of the optical rays escaping from the core, which suppresses the subsequent radiations to the far field by constituting some destructive interference [10]. The fiber performance is further improved by the nodeless cladding structure to form a free core boundary, which eliminates the additional optical loss in the transmission band [11]. Subsequently a single-mode guidance was achieved with a low bending loss [12,13]. Recently, a conjoined-tube HC-NCF [14] with ultralow loss and broad bandwidth was designed and fabricated by adding more anti-resonant layers in the cladding area. Despite the emerging cutting-edge research in fiber technology, the use of HC-NCF for gas sensing has not been fully investigated. In this letter, we demonstrate the sensitive detection of carbon monoxide (CO) at 2.3 μm by performing PTI in a custom-made HC-NCF.

The HC-NCF (85 cm in length) has a 40-μm air core that is surrounded by a single ring of eight nontouching capillaries.

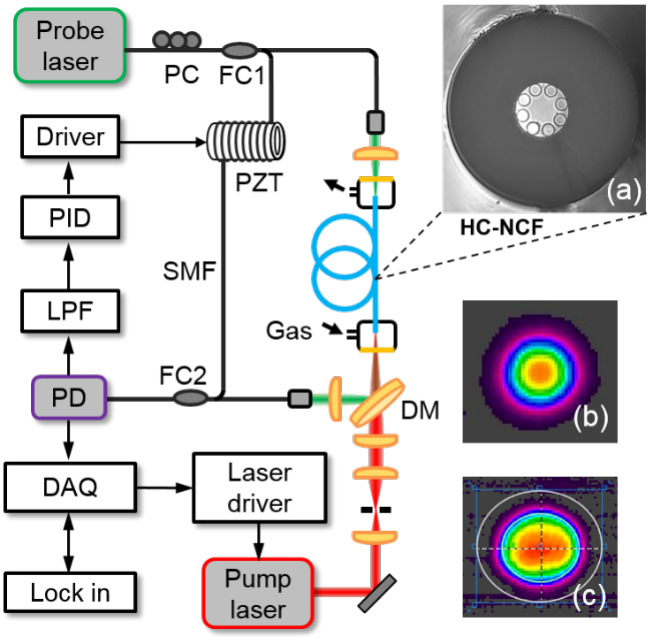

Fig. 1. Experimental setup of the PTI CO sensor using a HC-NCF. DM: dichroic mirror; FC: fiber coupler; PD: photodetector; PC: polarization controller; LPF: low-pass filter. (a) Micrograph of the HC-NCF cross section. (b) Beam profile of the pump laser transmitted through the HC-NCF. (c) Beam profile of the pump laser before being coupled into the HC-NCF.

As shown in Fig. 1(a), the capillaries form a node-less cladding structure to serve as a free core boundary. To enhance the coupling efficiency, we adopted the free-space coupling optics to direct the infrared laser beams at 2.3 μm and 1.5 μm both into the HC-NCF. In particular, by using a telescope system with a pinhole for beam shaping and a plano-convex lens (f = 50 mm), we achieved a coupling efficiency of 90% for the 2.3-μm pump laser. The mode field diameter (MFD) of the HC-NCF is estimated to be 0.63 of the core diameter. The proper fiber coupling and light delivery could be verified by the near-field imaging of the transmitted beam captured by a pyroelectric infrared camera. Fig. 1 illustrates the Gaussian beam profiles of the pump laser measured before and after passing through the HC-NCF.

Fig. 1 also depicts the schematic of the PTI CO sensor. A continuous-wave distributed feedback (DFB) laser at 2.3 μm serves as the pump laser. The DFB laser could be tuned between 4296 cm^{-1} and 4303 cm^{-1} by adjusting the injection current with an emission power up to 4.5 mW. The target CO line R(10) at 4297.7 cm^{-1} in the $2v_1$ band has an absorption line-strength of 2.937×10^{-21} $cm^{-1}/(molecule\cdot cm^{-2})$ at room temperature (296 K) [15]. The probe laser wavelength was selected to be 1533 nm using a tunable fiber-coupled diode laser. The output from the probe laser was split into two arms, sensing arm and reference arm, respectively to form a Mach-Zehnder interferometer (MZI) for the phase detection. The single-mode fiber in the reference arm was coiled around a piezo-electric transducer (PZT) phase modulator to make the MZI operate at the quadrature point using a fast-feedback servo loop. In the sensing arm, the probe laser and pump laser were both coupled into the HC-NCF. The two ends of the HC-NCF were enclosed in the gas cells that were used as the gas inlet and outlet, respectively. After exiting

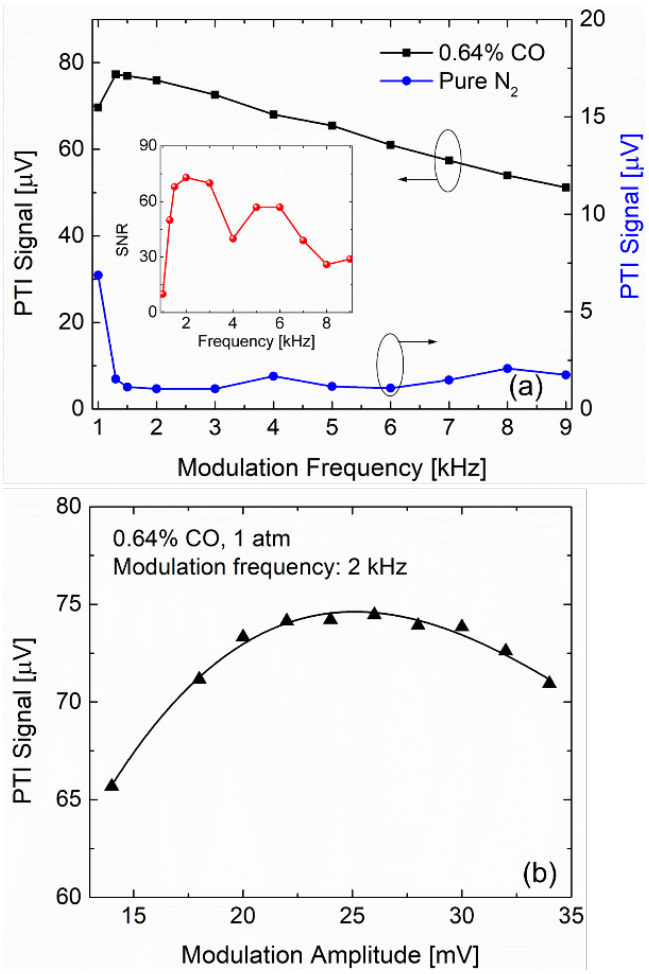

Fig. 2. (a) Dependence of PTI-2*f* signal (0.64% CO) and noise (N_2) on modulation frequency. The corresponding SNR is plotted in the inset graph. (b) PTI-2*f* signal as a function of modulation amplitude of the pump laser.

the HC-NCF, the probe laser was separated by a dichroic mirror and coupled into the single-mode fiber to be combined with the reference arm. A polarization controller was adopted for the probe light to maximize the interference fringe contrast.

The interferometric signal was detected by a photodetector followed by a lock-in amplifier to perform wavelength modulation spectroscopy with the second harmonic detection (WMS-2*f*). The pump laser wavelength was scanned (mHz) across the absorption line and modulated at a higher frequency (*f*, in kHz). The photothermal signal was demodulated at the second harmonic (2*f*) of the modulation frequency. A typical PTI-2*f* signal is proportional to the weak gas absorption and peaks at the absorption line-center.

The optimal modulation frequency and depth of the pump laser should be selected to maximize the signal-to-noise ratio (SNR). Fig. 2(a) presents the measured PTI-2*f* signal at the line-center of CO as a function of modulation frequency between 1 kHz and 9 kHz. The background noise is also plotted at the same modulation frequency by measuring pure N_2. All the measurements were conducted at atmospheric pressure. It is seen in Fig. 2(a) that the PTI signal increases almost linearly with the decreased modulation frequency but is gradually affected by the noise at the

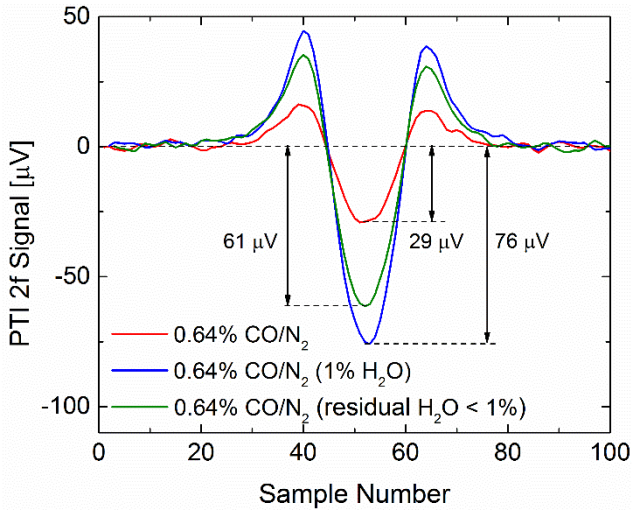

Fig. 3. Influence of H_2O additive on the PTI-2*f* signal of CO mixtures.

frequency below 1.3 kHz. The significant noise at low frequencies mostly comes from the 1/*f* flicker noise and other slow-varying noise in the ambient, whereas the noise at higher frequencies is likely associated with the PZT electronics. Thus we obtain the best SNR at a modulation frequency of 2 kHz.

The PTI-2*f* signal also depends on the modulation depth of the pump laser, which could be adjusted by varying the sinusoidal voltage applied to the laser driver. Fig. 2(b) plots the PTI-2*f* amplitudes measured at different modulation depths for the selected modulation frequency of 2 kHz. In this case, the optimal modulation voltage was found to be at 25 mV.

The photothermal process in the infrared involves the energy transfer from the ro-vibrational state of gas molecules to translational degrees of freedom via molecular collisions. This process is determined by the vibrational-translational (V-T) relaxation rate ($\tau_{v\text{-}t}$) of the gas. Due to the high modulation frequency of the pump laser, the heat generation rate of V-T relaxation may not follow the laser modulation rate, leading to a reduced photothermal signal compared with the case of a fast V-T energy equilibration. The direct V-T energy transfer of the excited CO in the bath gas N_2 is known to be an extremely slow process [16]. Actually, the observed photothermal signal in the dry CO/N_2 mixture is mostly caused by the fast rotation-relaxation of CO. The next fast process is the V-V energy transfer to N_2 vibration, but the V-T relaxation of N_2 is also known to be slow. Thus only a small portion of the excitation energy is transferred to photothermal signal in the dry CO/N_2 mixture. Most of the excitation energy is released by the irreversible leakage to N_2 and collision with the inner wall of the HCF.

The previous studies [16,17] have shown that the V-T relaxation of CO by molecular collisions with H_2O molecules is much faster than that of dry CO/N_2 mixtures. Thus we added water vapor to CO mixtures to promote the V-T relaxation and thus in order to enhance the PTI signal. Note that H_2O is naturally abundant and has no absorption interference at the pump and probe laser wavelengths. In the experiment, the HC-NCF was first purged with pure N_2, followed by the PTI detection of the dry mixture of 0.64% CO/N_2. In comparison, the dry CO mixture was then mixed with ambient air (relative humidity 65% at 23.5°C) to produce a mixture of 0.64% CO and 1% H_2O balanced by N_2. Fig. 3 compares the measured PTI-2*f* spectra of the two gas mixtures, showing an enhancement factor of 2.6 by the addition of H_2O. The phase angle of the lock-in amplifier was observed to shift by 7° between the two measurements, indicating the increased CO relaxation due to the presence of H_2O. Note that the phase change of the PTI signal results from the varying relaxation phase lag due to using the same electronic system. The PTI signal of CO could be affected by different amount of H_2O mixture. After measuring the mixture of 1% H_2O, we purged the fiber with pure N_2 for a short time so that some residual H_2O still existed inside the hollow core. Then, by filling 0.64% CO into the hollow core, the obtained PTI 2f amplitude shown in Fig. 3 is between that of the dry CO and that with 1% H2O additive.

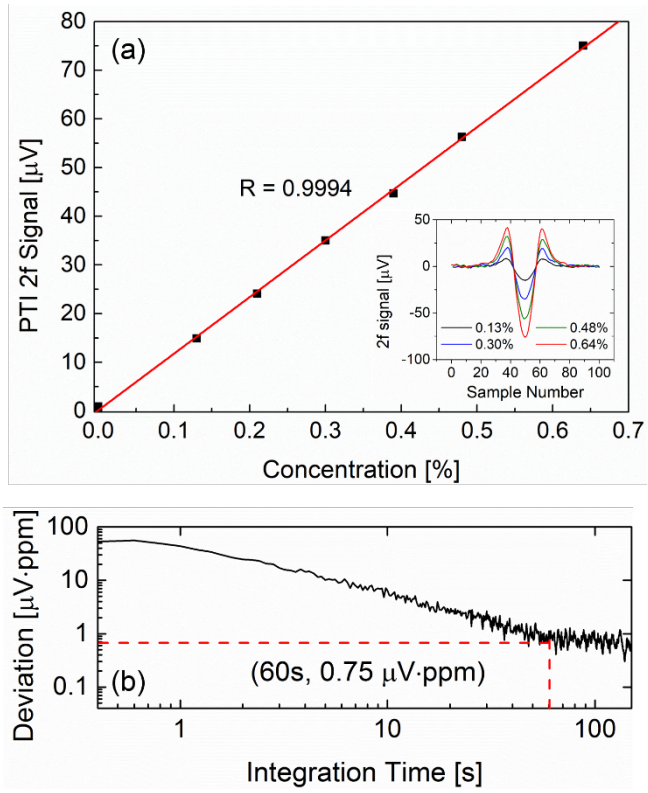

Fig. 4. (a) Linear response of the PTI sensor to CO concentration. Insert: representative PTI-2*f* signals at different CO concentrations. (b) Allan-Werle deviation (ppm) as a function of integration time (s).

Fig. 4(a) depicts the measured PTI-2f peak amplitude as a function of CO concentration with a constant 1% H_2O additive. The sensor calibration yields an excellent linear response with an R-square value of 0.9994. Based on the obtained sensor response and the 1σ noise, we obtained the noise equivalent concentration (NEC, SNR = 1) of 90 ppm, corresponding to 4.4×10^{-8} $cm^{-1}WHz^{-1/2}$ in the normalized noise equivalent absorption coefficient (NNEA) for a 0.8 Hz detection bandwidth and 1.1 mW pump power. The current NNEA is one order of magnitude better than the previous PTI sensor [7], which is mainly due to the smaller diameter of the hollow core used in this work. The Allan-Werle deviation analysis was conducted by measuring pure N_2 in the hollow core. The result in Fig. 4(b) shows the turning point at the integration time of 1 minute, leading to an improved CO sensitivity of 0.75 μV·ppm

Although this work demonstrates the first photothermal CO sensor, the detection of CO has been previously investigated by photoacoustic spectroscopy (PAS) including quartz-enhanced PAS (QEPAS) and evanescent-wave QEAPS (EW-QEPAS) in the mid-infrared [18–23]. The PAS sensors detect the acoustic waves

caused by the V-T energy transfer, where the sensor performance is relevant to laser power, V-T relaxation rate and gas pressure.

Table 1. Comparison of the PTI CO sensor with the state-of-the-art PAS CO sensors.

Technique	Pump λ [μm]	Pressure [bar]	NNEA [$cm^{-1}WHz^{-1/2}$]
PAS [18]	4.75	1	2.8×10^{-7}
QEPAS [19]	4.55	0.06	5.3×10^{-7}
QEPAS [20]	4.55	0.06	7.4×10^{-8}
QEPAS [22]	4.61	1	1.6×10^{-8}
EW-QEPAS [23]	2.327	1	8.6×10^{-8}
PTI (this work)	2.327	1	4.4×10^{-8}

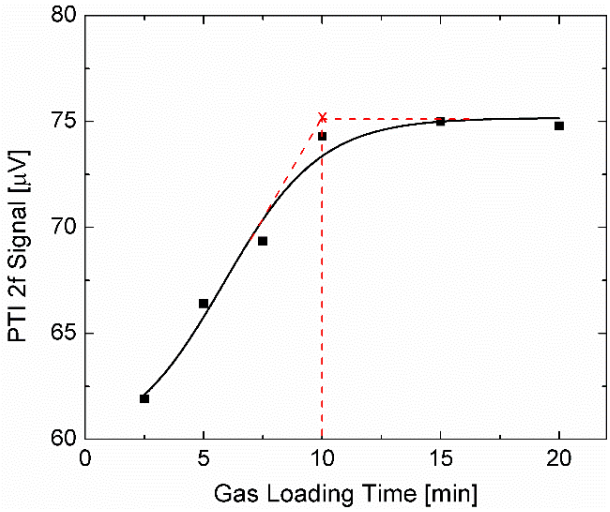

Fig. 5. Dependence of the measured PTI-2f signal on the gas loading time.

Table 1 compares the detection sensitivity of the current PTI CO sensor with that of the PAS sensors reported in the literature. Our PTI sensor using the HC-NCF demonstrates the comparative performance with the state-of-the-art PAS gas sensors.

The present PTI CO sensor loads the gas sample into the hollow core from the fiber end that is enclosed in a gas cell with a volume of 4.3 ml. We investigated the response time of the sensor by measuring the PTI signals at different time intervals. Fig. 5 shows the time-varied PTI signal when 0.64% CO was introduced into the HC-NCF. It is evident that after 10 min the PTI signal reaches a plateau level that agrees with the calibration curve shown in Fig. 4(a). Note that the gas exchange time could be further reduced using a higher pump pressure.

In summary, we reported the first PTI CO sensor using a HC-NCF. The pump laser at 2327 nm for CO excitation and the probe laser at 1533 nm were both coupled into the HC-NCF with a 40-μm core size. The HC-NCF-based PTI sensor achieves a NNEA of 4.4×10^{-8} $cm^{-1}WHz^{-1/2}$ and the minimum detectable concentration of 0.75 μV·ppm CO at 60-s integration time for the pump power as low as 1.1 mW. Because CO has a relatively slow V-T relaxation rate, we demonstrated the enhancement of the photothermal signal by adding water vapor to the gas mixture. Photothermal effect of molecules with a slow V-T relaxation rate in the small hollow core will be further explored at varying gas pressures. The combination of HC- NCF with photothermal spectroscopy enables sensitive gas detection in an extremely small sampling volume. Applications of the present sensing technique to other gaseous species or liquid samples are also of interest. It should be noted that conventional hollow-core photonic bandgap fibers only have transmission in the visible and near-infrared range. The HC- NCF could deliver light beyond 3 μm with a low-mode noise, making ultrasensitive mid-infrared gas sensing possible. Additionally, with the further advancement of mid-infrared optics, it is possible to use the proposed technique to realize mid-infrared all-fiber distributed sensing.

Funding. General Research Fund (14206317) of Research Grants Council (RGC) of Hong Kong SAR, China.

REFERENCES

1. M. A. Owens, C. C. Davis, R. R. Dickerson, Anal. Chem. **71**, 1391 (1999).
2. K. Krzempek, G. Dudzik, K. Abramski, Opt. Express. **26**, 28811 (2018).
3. F. Benabid, F. Couny, J. C. Knight, T. A. Birks, Nature **434**, 463 (2005).
4. W. Jin, Y. Cao, F. Yang, H. L. Ho, Nat. Commun. **6**, 1 (2015).
5. Y. Lin, W. Jin, F. Yang, Y. Tan, H. L. Ho, Opt. Lett. **42**, 4712 (2017).
6. Y. Zhao, W. Jin, Y. Lin, F. Yang, H. L. Ho, Opt. Lett. **43**, 1566 (2018).
7. Z. Li, Z. Wang, F. Yang, W. Jin, W. Ren, Opt. Lett. **42**, 3718 (2017).
8. F. Yu, J. Knight, IEEE J. Sel. Top. Quantum Electron. **22**, 1 (2015).
9. Y. Y. Wang, N. V. Wheeler, F. Couny, P. J. Roberts, F. Benabid, Opt. Lett. **36**, 669 (2011).
10. Y. Wang, W. Ding, Opt. Express. **25**, 33122 (2017).
11. A. N. Kolyadin, A. F. Kosolapov, A. D. Pryamikov, A. S. Biriukov, V. G. Plotnichenko, E. M. Dianov, Opt. Express. **21**, 9514 (2013).
12. W. Belardi, J. C. Knight, Opt. Express. **22**, 10091 (2014).
13. S.-F. Gao, Y.-Y. Wang, X.-L. Liu, W. Ding, P. Wang, Opt. Express. **24**, 14801 (2016).
14. S. Gao, Y. Wang, W. Ding, D. Jiang, S. Gu, X. Zhang, P. Wang, Nat. Commun. **9**, 2828 (2018).
15. I. E. Gordon, L. S. Rothman, C. Hill, R. V Kochanov, Y. Tan, P. F. Bernath, M. Birk, V. Boudon, A. Campargue, K. V Chance, B. J. Drouin, J.-M. Flaud, R. R. Gamache, J. T. Hodges, D. Jacquemart, V. I. Perevalov, A. Perrin, K. P. Shine, M.-A. H. Smith, et al., J. Quant. Spectrosc. Radiat. Transf. **203**, 3 (2017).
16. W. J. Hooker, R. C. Millikan, J. Chem. Phys. **38**, 214 (1963).
17. J. C. Stephenson, E. R. Mosburg Jr., J. Chem. Phys. **60**, 1 (1974).
18. R. Gerlach, N. M. Amer, Appl. Phys. Lett. **32**, 228 (1978).
19. A. A. Kosterev, Y. A. Bakhirkin, F. K. Tittel, Appl. Phys. B Lasers Opt. **80**, 133 (2005).
20. A. A. Kosterev, Y. A. Bakhirkin, F. K. Tittel, S. Blaser, Y. Bonetti, L. Hvozdara, Appl. Phys. B Lasers Opt. **78**, 673 (2004).
21. X. Yin, L. Dong, H. Zheng, X. Liu, H. Wu, Y. Yang, W. Ma, L. Zhang, W. Yin, L. Xiao, S. Jia, Sensors (Switzerland). **16**, 162 (2016).
22. Y. Ma, R. Lewicki, M. Razeghi, F. K. Tittel, Opt. Express. **21**, 1008 (2013).
23. Z. Li, Z. Wang, C. Wang, W. Ren, Appl. Phys. B Lasers Opt. **122**, 1 (2016).

Full references:

1. M. A. Owens, C. C. Davis, and R. R. Dickerson, "A photothermal interferometer for gas-phase ammonia detection," Anal. Chem. **71**, 1391–1399 (1999).
2. K. Krzempek, G. Dudzik, and K. Abramski, "Photothermal spectroscopy of CO2 in an intracavity mode-locked fiber laser configuration," Opt. Express **26**, 28811–28871 (2018).
3. F. Benabid, F. Couny, J. C. Knight, and T. A. Birks, Nature **434**, 463–466 (2005).
4. W. Jin, Y. Cao, F. Yang, and H. L. Ho, "Ultra-sensitive all-fibre photothermal spectroscopy with large dynamic range," Nat. Commun. **6**, 1–8 (2015).
5. Y. Lin, W. Jin, F. Yang, Y. Tan, and H. L. Ho, "Performance optimization of hollow-core fiber photothermal gas sensors," Opt. Lett. **42**, 4712 (2017).
6. Y. Zhao, W. Jin, Y. Lin, F. Yang, and H. L. Ho, "All-fiber gas sensor with intracavity photothermal spectroscopy," Opt. Lett. **43**, 1566 (2018).
7. Z. Li, Z. Wang, F. Yang, W. Jin, and W. Ren, "Mid-infrared fiber-optic photothermal interferometry," Opt. Lett. **42**, 3718 (2017).
8. F. Yu and J. Knight, "Negative Curvature Hollow Core Optical Fiber," IEEE J. Sel. Top. Quantum Electron. **22**, 1 (2015).
9. Y. Y. Wang, N. V. Wheeler, F. Couny, P. J. Roberts, and F. Benabid, "Low loss broadband transmission in hypocycloid-core Kagome hollow-core photonic crystal fiber," Opt. Lett. **36,** 669 (2011).
10. Y. Wang and W. Ding, "Confinement loss in hollow-core negative curvature fiber: A multi-layered model," Opt. Express **25**, 33122–33133 (2017).
11. A. N. Kolyadin, A. F. Kosolapov, A. D. Pryamikov, A. S. Biriukov, V. G. Plotnichenko, and E. M. Dianov, "Light transmission in negative curvature hollow core fiber in extremely high material loss region," Opt. Express **21**, 9514 (2013).
12. W. Belardi and J. C. Knight, "Hollow antiresonant fibers with low bending loss," Opt. Express **22**, 10091 (2014).
13. S.-F. Gao, Y.-Y. Wang, X.-L. Liu, W. Ding, and P. Wang, "Bending loss characterization in nodeless hollow-core anti-resonant fiber," Opt. Express **24**, 14801–14811 (2016).
14. S. Gao, Y. Wang, W. Ding, D. Jiang, S. Gu, X. Zhang, and P. Wang, "Hollow-core conjoined-tube negative-curvature fibre with ultralow loss," Nat. Commun. **9**, 2828 (2018).
15. I. E. Gordon, L. S. Rothman, C. Hill, R. V Kochanov, Y. Tan, P. F. Bernath, M. Birk, V. Boudon, A. Campargue, K. V Chance, B. J. Drouin, J.-M. Flaud, R. R. Gamache, J. T. Hodges, D. Jacquemart, V. I. Perevalov, A. Perrin, K. P. Shine, M.-A. H. Smith, J. Tennyson, G. C. Toon, H. Tran, V. G. Tyuterev, A. Barbe, A. G. Császár, V. M. Devi, T. Furtenbacher, J. J. Harrison, J.-M. Hartmann, A. Jolly, T. J. Johnson, T. Karman, I. Kleiner, A. A. Kyuberis, J. Loos, O. M. Lyulin, S. T. Massie, S. N. Mikhailenko, N. Moazzen-Ahmadi, H. S. P. Müller, O. V Naumenko, A. V Nikitin, O. L. Polyansky, M. Rey, M. Rotger, S. W. Sharpe, K. Sung, E. Starikova, S. A. Tashkun, J. Vander Auwera, G. Wagner, J. Wilzewski, P. Wcisło, S. Yu, and E. J. Zak, "The HITRAN2016 molecular spectroscopic database," J. Quant. Spectrosc. Radiat. Transf. **203**, 3–69 (2017).
16. W. J. Hooker and R. C. Millikan, "Study of vibrational relaxation in carbon monoxide for the fundamental and first overtone," J. Chem. Phys. **38**, 214–220 (1963).
17. J. C. Stephenson and E. R. Mosburg Jr., "Vibrational energy transfer in CO from 100 to 300 °K," J. Chem. Phys. **60**, 1–5 (1974).
18. R. Gerlach and N. M. Amer, "Sensitive optoacoustic detection of carbon monoxide by resonance absorption," Appl. Phys. Lett. **32**, 228–231 (1978).
19. A. A. Kosterev, Y. A. Bakhirkin, and F. K. Tittel, "Ultrasensitive gas detection by quartz-enhanced photoacoustic spectroscopy in the fundamental molecular absorption bands region," Appl. Phys. B Lasers Opt. **80**, 133–138 (2005).
20. A. A. Kosterev, Y. A. Bakhirkin, F. K. Tittel, S. Blaser, Y. Bonetti, and L. Hvozdara, "Photoacoustic phase shift as a chemically selective spectroscopic parameter," Appl. Phys. B Lasers Opt. **78**, 673–676 (2004).
21. X. Yin, L. Dong, H. Zheng, X. Liu, H. Wu, Y. Yang, W. Ma, L. Zhang, W. Yin, L. Xiao, and S. Jia, "Impact of humidity on quartz-enhanced photoacoustic spectroscopy based CO detection using a near-IR telecommunication diode laser," Sensors (Switzerland) **16**, (2016).
22. Y. Ma, R. Lewicki, M. Razeghi, and F. K. Tittel, "QEPAS based ppb-level detection of CO and N_2O using a high power CW DFB-QCL," Opt. Express **21**, 1008 (2013).
23. Z. Li, Z. Wang, C. Wang, and W. Ren, "Optical fiber tip-based quartz-enhanced photoacoustic sensor for trace gas detection," Appl. Phys. B Lasers Opt. **122**, 1–6 (2016).